2009-08

Hybrid Control of Long Endurance Unmanned Aerial Vehicles for Robust Wireless Sensor Networking

Lee, D.-J.

D.-J. Lee, K. Andersson, I. Kaminer, D. P. Horner, and K. D. Jones, "Hybrid Control of Long Endurance Unmanned Aerial Vehicles for Robust Wireless Sensor Networking", in Proceedings of AIAA Guidance, Navigation, and Control Conference, Chicago, IL,

AIAA Guidance, Navigation, and Control Conference
10 - 13 August 2009, Chicago, Illinois

AIAA-2009-6099

Hybrid Control of Long Endurance Unmanned Aerial Vehicles for Robust Wireless Communication Networking

Deok-Jin Lee[1], Klas Andersson[2], and Kevin D. Jones[3]
Naval Postgraduate School, Monterey, CA, 93943

This paper presents an effective hybrid control approach for building stable wireless sensor networks between heterogeneous unmanned vehicles using high endurance aerial vehicles. For optimal deployment of the aerial vehicles in communication networks, a gradient descent based self-estimating control algorithm is utilized to locate the aerial platforms to maintain maximum communication throughputs between distributed multiple nodes. The autonomous aerial robots, which function as communication relay nodes, harness thermal energy from the atmosphere to improve their flight endurance within specified communication coverage areas. The rapidly-deployable communication networks with the high-endurance aerial vehicles can be used for various application areas including environment monitoring, surveillance, tracking, and decision-making support. Flight test and simulation studies are conducted to evaluate the effectiveness of the proposed hybrid control technique for robust communication networks.

I. Introduction

In recent years, unmanned aerial vehicles (UAVs) have received significant attention in both military and civil applications. [1] In future wireless network-centric environments, teams of heterogeneous autonomous vehicles will be deployed in a cooperative manner to conduct wide-area sensing, surveillance, communication networking in various environments and a broad range of applications.[2] Coordinated autonomous operations by teams of heterogeneous vehicles such as aerial, surface, and underwater robots will increase the functionality of distributed sensing for shared situational awareness. In addition, sensor data analysis and integration would provide automated decision-making support, object detection, and mapping capabilities. The cooperative operations between the multiple autonomous vehicles using a UAV as a sensing and relaying agent are constrained by sensor range and communication limits, and operational environments.[4] In principle, wireless mesh networking between the vehicles can provide wide area coverage, and video and sensory data for situational awareness and surveillance. Under this operational concept, unmanned aerial vehicles play an important role of long-range sensors as relay communication relay nodes. Stable communication networking between a distributed autonomous system (DAS) of networked vehicle and sensing nodes as well as autonomy of the unmanned vehicles will be key technologies for high-performance and remote operation in these applications. Challenging tasks for successful communication networking between the DAS using the UAV as the flying sensing and relay node include real-time flight trajectory optimization, long operational range, and long flight endurance of the aerial vehicle to maximize the coordinated autonomous operations.

The concept of communication relay using UAVs was proposed in the literature[3] where the UAVs are used as platforms for a high capacity trunk radio relay and battlefield broadcast systems. More research has been conducted on this type of communication networks[5~8] but there are few flight experiments that have tried to realize this idea in actuality and succeeded in real test with flying aerial vehicles. Frew and his colleagues[6] have conducted research on this topic and developed a Lyapunov guidance vector field (LGVF) based control algorithm that takes gradient inputs from a perturbation-based extremum seeking approach in order to control the UAV positioning to optimize communication links. While, in Ref. 7, the optimal UAV position is calculated by maximizing the average data rate keeping the symbol error rate (SER) below a certain threshold. On the other hand, Lee and his colleagues[9] have demonstrated successful flight experiments for high bandwidth communication networks between distributed multiple nodes using aerial vehicles as communication relay nodes. In those flight experiments, self-estimating

[1] NRC Research Associate/Adjunct Research Professor, Dept. of Mech. & Astronautical Eng., member AIAA.
[2] Research Associate, Dept. of Mech. & Astronautical Eng., member AIAA.
[3] Research Associate Professor, Dept. of Mech. & Astronautical Eng., Associate Fellow AIAA.

extremum control techniques were developed in order to steer the aerial vehicles to obtain optimal flight trajectories which maximize wireless communication throughputs between ground user node and remote node.

For more sophisticated tasks, often teams of autonomous unmanned vehicles are deployed in a cooperative manner to cover wider area and to establish a robust communication networks in places where the infrastructure is damaged and absent, or in war theaters. The operational range of the unmanned vehicles, however, is usually limited by the communication range of communication systems.[5] To increase and allow stable real-time transmission of data back to the command control station, it is necessary to develop a real-time robust control algorithm that will force the networked autonomous vehicles to reposition themselves autonomously to maintain an optimal loitering flight path that will maximize the signal throughputs of the communication links between the heterogeneous vehicles including the ground control station.[9] In addition, there are limited onboard energy power sources in small and micro unmanned aerial vehicles, which results in reduced endurance and range.[10] Additionally, low Reynolds numbers that are inherent to small or micro UAV make it difficult to attain an efficiency comparable to larger aircraft. Typically, small or micro aerial vehicles have flight durations from to 1 to 2 hours even with advanced technology in the aerial platform design, thus it is required to develop advanced technologies to improve the flight endurance for small and micro aerial vehicles. [11]

The objective of this research aims at building robust wireless communication networks by using small UAVs whose flight endurance is improved by using convective energy from the atmosphere. There are two challenging issues to overcome to turn this idea into reality. The first issue is to how to control the UAVs to be located at optimal communication relay area, and second question lies on the method of extending flight endurance of the small aerial vehicles that use thermals. For distributed networked communication nodes, the location of each UAV is continuously adjusted by a distributed control algorithm building beyond line-of-sight transmission between UAVs as well as remote users.

As a solution to the first issue, optimal location of the small UAVs is calculated by applying a real-time optimal searching technique which is based on a gradient descent numerical optimization approach.[9] The cost function used in the on-line optimization architecture for the UAV localization control is based on the signal-to-noise ratio (SNR) that is provided from an antenna propagation model. Additionally, as a strategy to achieve high endurance for small UAVs, autonomous gliders that extract energy from the environment by autonomously seeking thermal lift will be deployed with the proposed onboard soaring control technique[12]. This extra energy will supplement the onboard fuel supplies and thereby extend the maximum endurance of the UAV. The technique is the same as glider pilots use to extend their time in the air. Studies have been conducted on the subject[10-15] of using either static or dynamic soaring energy to sustain flight, but a few have tried to realize this idea in actuality and tested it in flight[11,12]. In this paper, the soaring control technique adopted by Andersson and colleagues is utilized to extend the flight endurance of an autonomous UAV, which plays an essential role for keeping robust communication and data relay between distributed multiple users without loss of communication.

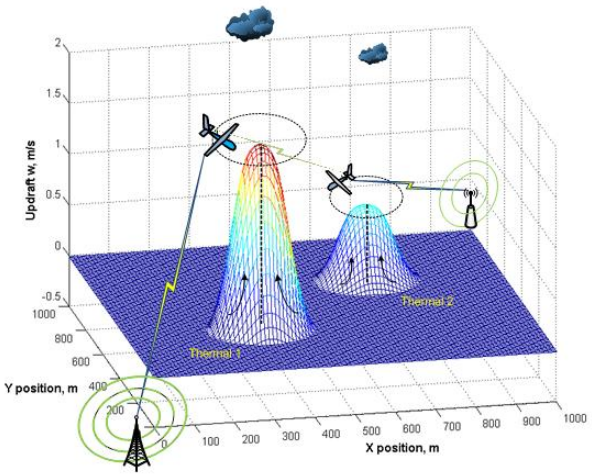

Figure 1 Hybrid Control of High-Endurance Unmanned Aerial Vehicles for Robust Communication Networks

In this paper, a synthesized hybrid control technique which integrates two efficient control algorithms is proposed to obtain the goals. Initially, the motion of each UAV is controlled by the self-estimating extremum controller[9]. This guides the UAV to reach the optimal location that provides the highest communication throughput.

The autonomous thermal soaring control algorithm[12] is then executed to harness energy to minimize the fuel consumption within a specified region. If the communication signal strength falls below a certain threshold value, the control node is switched back to the extremum control mode. The overall concept of the synthesized switching control methodology is illustrated in Fig. 1. In this paper, not only a theoretical technique which continuously steers the UAV positioning at the optimal location is proposed, but also flight test results are presented to verify the effectiveness of the proposed methods, which makes a unique distinction from other approaches in this sensor networks research. The performance of the proposed real-time gradient descent extremum controller is evaluated by conducting field experiments within the USSOCOM-sponsored Tactical Network Topologies (TNT) Cooperative Field Experimentation Program to measure the received signal strength of the wireless links sensed by each network node[9]. For flight tests, commercially-available broadband mobile ad-hoc networking (MANET) equipment for both stationary and mobile nodes within a localized wireless infrastructure was used. Moreover, the hybrid control technique integrated the soaring flight control technique into the self-estimating extremum control is verified through simulation studies with application to high bandwidth communication networking problem.

The remainder of this paper is organized as follows. Section II describes the overview of a hybrid control of a long-endurance unmanned aerial vehicle which uses a soaring flight technique to harness energy from the environment. Section III describes the self-estimating extremum control technique for optimizing the flight trajectory of an uninhabited aerial vehicle to obtain maximum communication links between multiple nodes. Section IV discusses the static soaring flight technique to extend the flight endurance of a small aerial vehicle. Section V presents flight test results. Finally, conclusion and discussion is presented in section VI.

II. Hybrid Control for Bio-Inspired Long Flight Endurance

In future network-centric environments, teams of autonomous unmanned vehicles will be deployed in a cooperative manner to cover wider area.[4] Depending on the objectives of the mission the goal could be either to maximize the distance covered during the flight, or the total time spent airborne. The operational range of the vehicles is usually restricted by range constraints of the communication systems or limited endurance of the aerial platforms used. For data and communications relay tasks the endurance of the aerial platforms is of special importance to make these missions more effective. Since the purpose for this paper is to maximize the loitering time at a location where the UAV can act as an effective communication relay node, the focus will be on trying to maximize endurance over a limited area rather than extending the maximum range. A hybrid control technique is developed for a stable communication relay with a small aerial vehicle, and the concept is described in Fig. 2. The hybrid control is designed by combining the self-estimating extremum controller[9] for a high bandwidth communication relay and the long-endurance flight controller[12] for a soaring technique for maximum flight endurance.

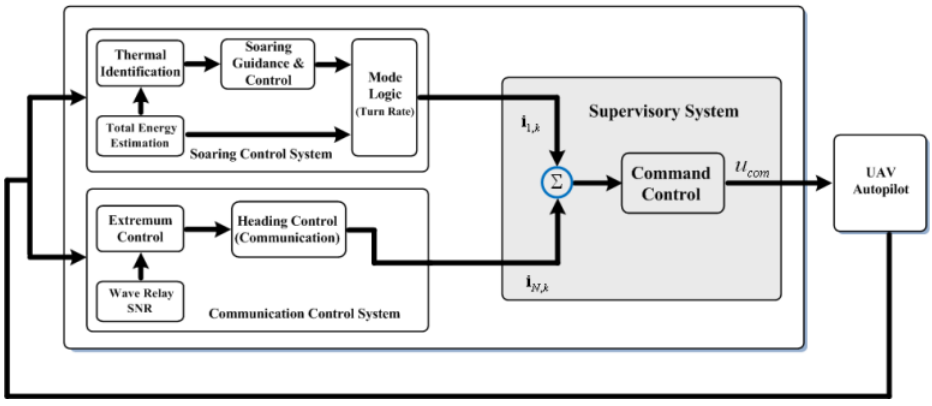

Figure 2 Control Synthesis for Soaring and Communication Control

Initially, the location of each UAV is controlled by the self-tuning extremum controller to steer an UAV to locate an optimal trajectory to guarantee high bandwidth communication links between a ground control center and a remote node. After the UAV reaches the optimal location which provides a high communication throughput, an area is designated in which the UAV is allowed to execute the soaring control algorithm. The glider will fly inside the limited area in search for thermals and when a thermal is found the UAV tries to circle within the updraft to gain

altitude. If the communication signal strength falls below a certain threshold value, the control is switched back to the extremum-seeking mode until the optimal communication-relay position is reestablished. This is done by using a supervision control system which has a decision-making capability, depicted in Fig. 2. The overall control is outer loop architecture which controls an autopilot onboard a UAV.

As the autonomous soaring glider is commanded to execute the onboard soaring-searching control algorithm, it flies in a spiral search pattern. The spiral flying is for thermal searching within a specified area where the limit of the area is determined by a minimum threshold value of the communication signal strength such as a signal-to-noise ratio (SNR). The spiral flying pattern for thermal energy is illustrated in Fig. 3 where the flying center $(\hat{x}_{opt}, \hat{y}_{opt})$ is the estimate of the optimal location of an aerial vehicle which guarantees the highest communication throughputs between multiple nodes. The maximum searching radius, R_{SNR}, is determined by solving the communication cost function of a predefined threshold SNR value. After the communication control mode is switched to the energy searching mode, onboard soaring control algorithms are executed to make the UAV fly in a specified spiral motion until it detects a thermal updraft. If the UAV reaches the maximum radius barrier, it returns to the optimal centering location and resume the thermal searching function.

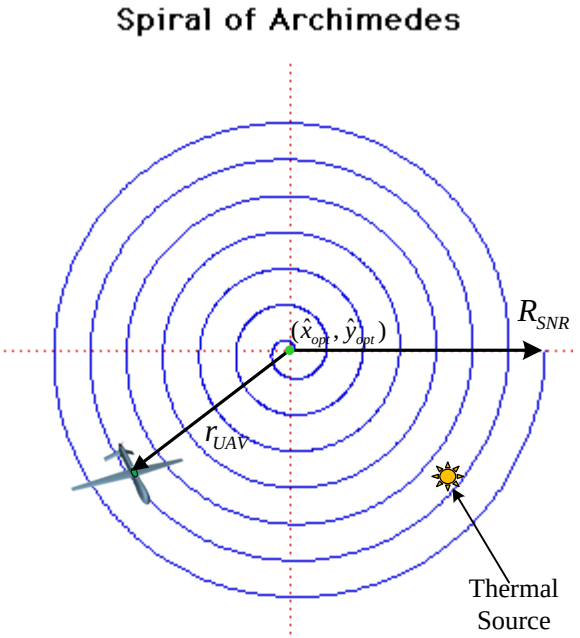

Figure 3 Spiral Flying Pattern Control for Soaring Searching with Spiral UAV Motion with respect to Maximum Communication Location

III. Self-Estimating Extremum Control for High Bandwidth Communication Links

In this section, a self-tuning extremum control algorithm is described, which allows the aerial relay vehicles to reposition themselves autonomously to maintain an optimal loitering flight path that maximizes the quality of the communication link between a command station and a remote user vehicle. The control algorithm for the optimal localization of a small UAV is developed by integrating a hill-climbing extremum control with a derivative-free gradient estimation algorithm which numerically computes the on-line gradient values of the SNR cost function as the figure of merit. [9] The overall structure of the proposed self-estimating extremum controller is illustrated in Fig. 4. The on-line estimation of the gradient of a performance function is achieved by utilizing a peak-seeking technique[16], which is a derivative-free recursive estimator that does not require specific knowledge of a mathematical model of a performance function. The aim of the self-tuning control algorithms is to build a robust controller combined with on-line gradient-seeking identifier. The technical motivation is that analytical gradient-type optimizers cannot be

applied to the problems where there is no knowledge of the derivatives of the system performance index. The function of each element in the self-estimating extremum control will be described below.

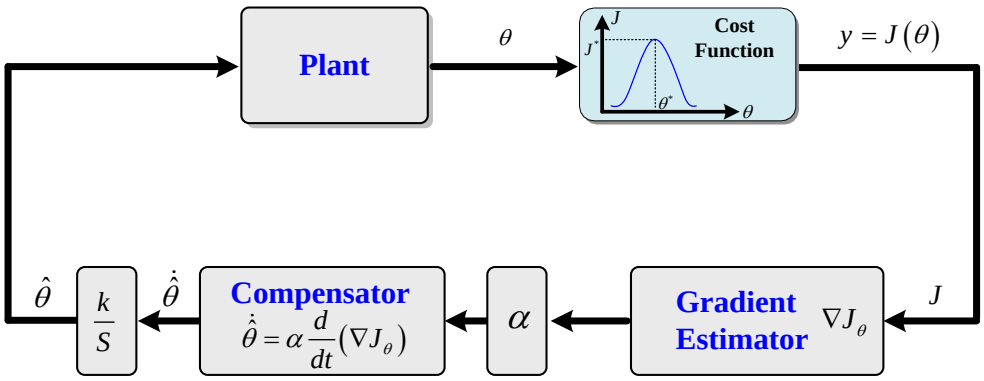

Figure 4 Self-Estimating Extremum Control Architecture

A. Gradient Descent Extremum Control Algorithms

The principle behind the gradient based optimization methods lies in the fact that an extremum has a gradient with the magnitude of zero.[17] To reach the objective, it is necessary for an objective function to be a smooth function with known parameters, and if noise is present in the cost function then it is necessary to have a good estimate of the gradient by applying a filter. Furthermore, if a mathematical model of the cost function is not available, the gradient computation is not trivial in optimization control applications. As an alternative way of computing the gradient of a cost function, the extremum-seeking approach that provides quantitative gradient value of the cost function in a numerical way is applied. In this section, a hill-climbing extremum control is reviewed.

Assume that the nonlinear dynamic and measurement model is given by

$$\begin{aligned} \mathbf{x}_{k+1} &= \mathbf{f}(\mathbf{x}_k, \mathbf{u}_k) \\ y_k &= J_k(\mathbf{x}_k) \end{aligned} \tag{1}$$

where $\mathbf{x}_k \in \Re^n$ is the n-dimensional state, given $\mathbf{f}: \Re^n \to \Re^n$, $\mathbf{u}_k \in \Re^l$ is the control input, and $y_k \in \Re$ is a scalar measurement cost function with $J: \Re^n \to \Re$. Based on the measurement of the system state, and cost function values, the peak-seeking controller is expected to regulate the state as guided by the search sequence, and in turn minimizes the performance output. Then, the peak-seeking control problem is interpreted as

$$\min_{x_k \in D} J_k(\mathbf{x}_k) \quad \text{subject to } \mathbf{x}_{k+1} = \mathbf{f}(\mathbf{x}_k, \mathbf{u}_k) \tag{2}$$

Consider a gradient based search method such as the steepest descent approach. Each iteration of a search loop computes a direction of the state. The search provides the following[18]

$$\mathbf{x}_{k+1} = \mathbf{x}_k + \alpha_k \mathbf{d}_k = \mathbf{x}_k - \alpha_k \mathbf{B}_k \mathbf{H}_k^{-1}(\mathbf{x}_k) \nabla J(\mathbf{x}_k) \tag{3}$$

where $\mathbf{d}_k \equiv -\mathbf{B}_k \mathbf{H}_k^{-1}(\mathbf{x}_k) \nabla J(\mathbf{x}_k)$ decides the direction of the search and is required to be a descent/ascent direction which allows the cost function J_k to be either reduced or increased gradually along the direction, and $\alpha_k > 0$ is the step length along the direction $\mathbf{d}_k$ and is a positive value which decides the convergence speed. $\mathbf{B}_k$ is a suitable approximation of the Hessian matrix $\mathbf{H}_k(\mathbf{x}_k) \equiv \nabla^2 J(\mathbf{x}_k)$, and $\mathbf{B}_k = \mathbf{I}$ is for the gradient method. Different choices of the direction vector $\mathbf{d}_k$ correspond to different methods. For the Gauss-Newton method, the direction is computed by

$$\mathbf{d}_k = -\mathbf{H}_k^{-1}\left(\mathbf{x}_k\right)\nabla J\left(\mathbf{x}_k\right) \tag{4}$$

where $\mathbf{H}_k$ is a positive definite Hessian matrix given by

$$h_{ij}(\mathbf{x}_k) = \frac{\partial^2 J}{\partial x_{i,k}\partial x_{j,k}}(\mathbf{x}_k), \quad i, j = 1,\ldots,n \tag{5}$$

The gradient method or steepest descent method sets the gradient direction to be

$$\mathbf{d}_k = -\mathbf{B}_k^{-1}\nabla J\left(\mathbf{x}_k\right) \tag{6}$$

In this paper, the gradient ascent method will be utilized by using Eqs. (3) and (6).

B. On-Line Gradient Estimation Using Peak-Seeking Approach

Now consider a way of estimating the gradient of a cost function. The maximization of the communication links between heterogeneous unmanned vehicles could be accomplished by maximizing the signal-to-noise ratio (SNR) between them. However, the function of the SNR value is not known in general, and thus it is difficult to apply directly an optimization technique, which is based on an analytical expression of the gradient of the cost function, to find an optimal location for the relay UAV. As promising solutions to the optimization without knowledge of the cost functional model, a perturbation-based extremum/peak seeking technique[17,19] is adopted. The perturbation-based peak-seeking approach is an adaptive optimization algorithm designed to drive the set point of a dynamic system to an optimal one, which provides quantitative gradient value of the cost function in a numerical way as inputs to the gradient descent based controller.

A typical peak-seeking structure is described in terms of the following four components where a high-pass filter plays a role of taking the gradient of the cost function and gives the rate of change of the cost function, and a low-pass filter takes out high frequency noise terms from the cost signal. For a further detailed illustration, suppose a general map function

$$y = J\left(\theta\right) \tag{7}$$

where $\theta \in \Re$ is an adjustable parameter, and $y \in \Re$ is the performance output, and $J : \Re \to \Re$ is an extremum around the extremum value $\theta^* \in \Re$. The objective of an extreme seeking mechanism is to steer θ to θ^* in real-time such that the cost function reaches the extremum $J^* = J\left(\theta^*\right)$. In order to seek the extremum, the cost function is perturbed locally around the current value of the parameter θ with a sinusoidal periodic signal, and uses the corresponding change of the objective output to estimate its local gradient. The gradient estimate is then used to update the parameter. If $\hat{\theta}$ is assumed to be the current value of the parameter, and $a\sin wt$ is a small sinusoidal perturbation around $\hat{\theta}$, then the output of the objective function is expressed by[16]

$$y = J\left(\hat{\theta} + a\sin wt\right) \approx J\left(\hat{\theta}\right) + a\left.\frac{\partial J}{\partial \theta}\right|_{\theta=\hat{\theta}} \sin wt \tag{8}$$

The constant term in the output y is removed by applying a high-pass filter (HPF) as a differentiator

$$y_H \approx a\left.\frac{\partial J}{\partial \theta}\right|_{\theta=\hat{\theta}} \sin wt \tag{9}$$

Demodulating y_H with a sinusoidal signal $\sin wt$ divides the signal into a low-frequency signal and a high-frequency signal

$$\varsigma = \frac{1}{2} a \left.\frac{\partial J}{\partial \theta}\right|_{\theta=\hat{\theta}} - \frac{1}{2} a \left.\frac{\partial J}{\partial \theta}\right|_{\theta=\hat{\theta}} \cos 2wt \tag{10}$$

Low-pass filtering of the demodulated the signal, ς, provides an estimate of the local gradient of $J(\theta)$

$$y_L \approx \frac{1}{2} a \left.\frac{\partial J}{\partial \theta}\right|_{\theta=\hat{\theta}} \tag{11}$$

The estimated gradient can be expressed in terms of the parameter change and

$$\dot{\hat{\theta}} = k \frac{1}{2} a \left.\frac{\partial J}{\partial \theta}\right|_{\theta=\hat{\theta}} \tag{12}$$

where k is a parameter to be selected. Since the objective function is assumed to be a smooth quadratic type function with an extremum value around the set point, it can be expressed by

$$J(\theta) = J(\theta^*) + \frac{1}{2} J''(\theta^*)\left(\hat{\theta} - \theta^*\right)^2 \tag{13}$$

Then, the gradient can be approximated locally around θ^* as

$$\nabla J_{\hat{\theta}} = \left.\frac{\partial J}{\partial \theta}\right|_{\theta=\hat{\theta}} \approx J''(\theta - \theta^*) \tag{14}$$

Denote $\tilde{\theta} = \hat{\theta} - \theta^*$ the convergence error, and taking a derivative of the error leads to $\dot{\tilde{\theta}} = \dot{\hat{\theta}}$. Then the differential equation of the error can be computed by

$$\dot{\tilde{\theta}} \approx k \frac{1}{2} a J''(\theta^*) \tilde{\theta} \tag{15}$$

which becomes stable with theproper choice of the parameters, a and k, i.e., $kaJ''(\theta^*) < 0$. Thus, the error $\tilde{\theta}$ converges asymptotically to the extremum point θ^*, at least locally around θ^*. The criterion for selecting the perturbation frequency is that it should be sufficiently higher than the cut-off frequencies of the low-pass and high-pass filters used in estimating the cost gradient.

C. UAV Heading Controller Design

Now consider designing the self-estimating extremum optimizer[9] which regulates the UAV reaching the optimal location by integrating the gradient-based hill climbing optimization algorithm in Eq. (3) with the gradient estimator of the extremum seeking approach in Eq. (12). The previously explained gradient estimation of a performance function is achieved by utilizing the peak-seeking approach, which is a numerical estimator and does not require specific knowledge of a mathematical model of a performance function.

For this model development, let assume that $\mathbf{p}(t) = [x(t), y(t), z(t)]^T$ present the UAV trajectory resolved in the local tangent coordinates (East, North, Down) as

$$\begin{aligned} \dot{x}(t) &= v \cos\psi \\ \dot{y}(t) &= v \sin\psi \\ \dot{\psi}(t) &= v\kappa \end{aligned} \tag{16}$$

where v is the speed of the UAV, ψ is the heading command, and κ is a bounded curvature. The control inputs can be the heading and the speed, but in this work it is assumed that the speed is constant. The commanded control input to the UAV is the only heading rate. The relation of the heading and the bank angle is represented by

$$\begin{aligned}\phi &= \tan^{-1}\left(\frac{v^2}{gR}\right) \\ &= \tan^{-1}\left(\frac{v}{g}\dot{\psi}\right)\end{aligned} \tag{17}$$

where the R is the radius of a curvature, and have the relationship with the speed and the heading rate, $v/R = \dot{\psi}$. The heading is defined as the heading of the UAV with respect to the positive *x*-axis.

The variations of the SNR performance function are a nonlinear function of several variables such as the relative distance between the UAV and the remote node and attitude of the UAV in flight. In this paper, for simplicity, it is assumed that the UAV has a constant speed with constant level flight ($\dot{h}(t) = 0$, where *h* is the altitude above the mean sea level) as shown in a UAV motion. In this case, the heading angle or bank angle is the only control variable, and the commanded control input is only a heading rate command, $u_{com}(t) = v\kappa = \dot{\psi}_{com}(t)$. If it is assumed that the ascent direction of $\mathbf{q}_k$ is equal to $\mathbf{q}_k = \nabla J(\mathbf{x}_k)$, then this gradient computation requires 2-dimensional gradient calculation. Now, using the fact that the components of the UAV position vector is an implicit function of the heading angle based on Eq. (16), $x(t) = f_1(\psi(t)), y(t) = f_2(\psi(t))$, the cost function in the optimization can be written as an implicit function of the heading angle only, $J(x(t), y(t), h(t)) = J(\psi(t))$, which reduces the multiple dimension of the gradient calculation to a scalar parameter. Specifically, following the gradient-based steepest descent approach, the descent direction of $\mathbf{d}_k$ becomes equal to $\mathbf{d}_k = \nabla J(\mathbf{x}_k) = \partial J / \partial \psi$, and the gradient of the cost function is obtained by using the numerical extremum-seeking approach instead of applying a direct analytical derivation method. Then the heading control can be decided by utilizing the gradient method by replacing the general state vector with the heading angle $\mathbf{x}_k \equiv \psi_k \in \Re^1$ as

$$\psi_{k+1} = \psi_k + \alpha_k \nabla J_\psi \tag{18}$$

where α_k is the step-length parameters which can be either constant or time-varying, and it is assumed that the gradient term, $\nabla J_\psi = \partial J / \partial \psi \in \Re$, can be obtainable from the peak-seeking approach explained in the previous subsection. Now rearranging the above equation gives

$$\begin{aligned}\psi_{k+1} - \psi_k &= \alpha_k \nabla J_\psi \\ \nabla \psi &= \alpha_k \nabla J_\psi\end{aligned} \tag{19}$$

Assuming the variation of the heading angle and the cost function at each time is small, and taking the derivative of the variation terms on both sides of Eq. (19) leads to the following relation

$$\frac{d\psi(t)}{dt} = \alpha(t)\frac{d}{dt}\left(\nabla J_\psi\right) \tag{20}$$

Now, suppose that the characteristics of the figure of merit of the cost function is quadratic in terms of the heading angle variable, then the performance function can be expressed by

$$J\left(\hat{\psi}(t)\right) = J^* + \frac{\mu}{2}\left(\hat{\psi}(t) - \psi^*\right)^2 + w(t) \tag{21}$$

where J^* is the maximum attainable value of the cost function, ψ^* is the heading angle which maximizes the performance function, $\hat{\psi}(t)$ is the current heading angle estimate, and μ is the sensitivity of the quadratic curve which relates heading angle to the indicated SNR, and $w(t)$ is a zero-mean white noise term which can be filtered out by applying a low-pass filter. It is assumed that the parameters which characterize the optimum values are unknown, but constant parameters. Taking a gradient of the cost function with respect to the current estimate $\hat{\psi}(t)$ provides the following

$$\nabla J_{\hat{\psi}(t)} \equiv \frac{\partial J\left(\hat{\psi}(t)\right)}{\partial \hat{\psi}(t)} = \mu\left(\hat{\psi}(t) - \psi^*\right) \tag{22}$$

Taking a time derivative of the above gradient term again leads to

$$\frac{d}{dt}\left(\nabla J_{\hat{\psi}(t)}\right) = \mu\left(\dot{\hat{\psi}}(t)\right) \tag{23}$$

Finally, substituting Eq. (23) into Eq. (20) gives the heading-rate control input as

$$\begin{aligned} \dot{\psi}_{com}(t) &= \frac{d\psi(t)}{dt} = \alpha(t)\frac{d}{dt}\left(\nabla J_{\psi}\right) \\ &= \mu\alpha(t)\dot{\hat{\psi}}(t) \end{aligned} \tag{24}$$

Note that the rate of the estimate of the current heading angle $\dot{\hat{\psi}}(t)$ can be obtained from Eq. (12) after applying the low-pass filter in the process of the extremum-seeking loop. We showed that the real-time heading-rate command for the control input to the autopilot of the UAV is calculated by integrating Eq. (24) with the heading-rate term produced from the extremum-seeking approach.

At the final stage of the extremum control approach when the UAV reaches the optimal location, it is necessary to make the UAV fly around the set point rather than fly directly to the point or pass over the point. Thus a steady-state heading $\dot{\psi}_{ss}$ is introduced to guarantee that the UAV will orbit with a constant radius R_{ss} at the final stage. The heading-rate command is expressed by

$$\dot{\psi}_{com} = \dot{\psi}_{ss} + \mu\alpha(t)\dot{\hat{\psi}}(t) \tag{25}$$

where ψ_{ss} is a steady-state heading input to be selected and is related to a final approach circle radius, $R_{ss} = v/\dot{\psi}_{ss}$. The time rate of change of the estimated heading angle is provided from the extremum seeking stage. Finally, the control input $u(t) \equiv \dot{\psi}_{com}(t)$ to the UAV is expressed by[8]

$$u(t) = \begin{cases} \dot{\psi}_{com}(t) = \dot{\psi}_{ss} & \text{if } \left|\dot{\psi}_{com}(t) - \dot{\psi}_{ss} = v/R_{ss}\right| \le \varepsilon_{ss} \\ \dot{\psi}_{com}(t) = \dot{\psi}_{ss} + \mu\alpha(t)\dot{\hat{\psi}}(t) & \text{other} \end{cases} \tag{26}$$

where ε_{ss} is a criterion which guarantees the bounded motion of the UAV at the final stage. This heading control input regulates the UAV system to follow the ascending direction of the cost function value until the UAV reaches the maximum point of the cost function. Once the UAV gets close to the optimal set point, it switches to a steady-state heading control mode to orbit around the optimal point with a predefined constant radius.

D. Adaptive Convergence Control

The computation of the adaptive time step α_k is based on the assumption that it is necessary for the cost function to be a sufficient decrease criterion. If the cost function is subject to unknown disturbances or noises, the computation of the gradient is no longer trivial. In this section, instead of calculating the condition directly, the

adaptive time-step scaling factor α_k is computed by using a more intuitive method. If the time rate of the gradient value of the SNR cost function $\Delta J_{k+1} = J_{k+1} - J_k$ or $d(\nabla J_{\hat{\psi}(t)})/dt$ is greater than τ_{tv} : a specified threshold value, the time-step scale factor is kept either the same as the previous one or scaled up by multiplying a third parameter $\gamma \geq 1$, $\Delta J_{k+1} \geq \tau_{tv}$, $\alpha_{k+1} = \alpha_k \times \gamma$. On the other hand, if the change of the gradient value of the SNR is smaller than the threshold value, the time-step is scaled down by multiplying a third scale factor $0 < \gamma < 1$, $\Delta J_{k+1} < \tau_{tv}$, $\alpha_{k+1} = \alpha_k \times \gamma$, which allows the UAV to have an almost straight flight path. In this way, the adaptive time-step α_k is computed by[9]

$$\alpha_{k+1} = \gamma \alpha_k, \text{ where } \begin{cases} 0 < \gamma < 1, & if \ \Delta J_{k+1} > \tau_{tv} \\ \gamma \geq 1, & else \ \Delta J_{k+1} < \tau_{tv} \end{cases} \tag{27}$$

where $\Delta J_{k+1} \equiv J_{k+1} - J_k$. This algorithm not only provides fast convergence properties but also reduces the unnecessary repeated circular motion of the UAV, which results from a direct searching mode to the optimal location.

E. Objective Functions for Communication

In most communication network systems, it is desirable to maximize the received signal power. The link quality of the communication network is dependent on the received signal power as well as the noise level of the system. Signal-to-noise ratio (SNR) is defined as a measure of the ratio between the received power and the noise power[12]. The higher the SNR, the larger the signal level as compared to the noise level, which result in a lower bit error rate in signal reception and means better link quality. According to the Shannon-Hartley theorem[20,21], the theoretical maximum channel capacity (*C*, in bits per second) is proportional to the SNR and the bandwidth (*W*, Hz) of the channel as

$$C = W \log_2(1 + SNR) \tag{28}$$

Assuming that the capacity of the channel is fully utilized, an increase in SNR will lead to an increase in the throughput of the channel. There are various sources of noise in the communication system which can come from the nature environment, system devices, and movement and orientation of the transmitter and receiver. Generally the mechanisms behind electromagnetic wave propagation are diverse, but can be attributed to direct line-of-sight (LOS) path, deflection, reflection, and scattering.[20]

In this section, a communication propagation model is developed to predict the signal-to-noise ratio (SNR) of the communication links, which is used as a reference SNR signal for the inputs to a feedback controller that is based on a real-time self-tuning extremum control approach. The propagation model is also used to analyze the variation of free-space propagation loss, antenna pattern loss, and the effect of UAV orientation on the signal-to-noise ratio in the communication link.[20] First, the free space path loss, which represents signal attenuation as a positive value measured in dB, is model as the difference between the transmitted power and the received power. The formula is based on Friis transmission formula[20], which is one of most dominant pass loss features affecting wave propagation in the radio channel.

The path loss model computes the path loss in dB between the UAV and ground relay nodes. The model for the path loss formula is based on Friis transmission formula and is expressed by

$$L_p(dB) = 32.4 + 20\log(f) + 20\log(d(t)) \tag{29}$$

$$d(t) \equiv \|\mathbf{d}(t)\| = \sqrt{\left(x(t) - x_{node,i}\right)^2 + \left(y(t) - y_{node,i}\right)^2 + \left(z(t) - z_{node,i}\right)^2} \tag{30}$$

where f is a frequency in MHz and $d(t)$ is distance in km.

The link budget model computes the received power, the signal-to-noise ratio (SNR) and link margin of the receiver. The equations for the link budget are given by[9]

$$P_r(dBm) = P_t(dBm) + G_t(dB) + G_r(dB) - L_p(dB) - L_{ap}(dB) \tag{31}$$

$$\text{Link Margin}(dBm) = P_r(dBm) - R_{sen}(dBm) \tag{32}$$

$$\text{SNR}(dBm) = \frac{P_r(dBm)}{P_n(dBm)} = \left(\frac{\lambda}{4\pi\|\mathbf{d}(t)\|}\right)^2 \frac{G_t G_r}{L_{ap}(t)} \tag{33}$$

where $P_r(dBm)$ is the receiver power, $P_t(dBm)$ is the transmitter power (28dBm), $R_{sen}(dBm)$ is the receiver sensitivity (-74 dBm), $G_t(dB)$ is transmitter antenna gain (14 dB), $G_r(dB)$ is receiver antenna gain (2.2 dB), $L_p(dB) \equiv (4\pi\|\mathbf{d}(t)\|/\lambda)^2$ is path loss which denotes the loss associated with propagation of electromagnetic waves, $L_{ap}(dB)$ is antenna pattern loss, $P_n(dB)$ is noise power (-95 dBm), $P_{sen}(dBm)$ is receiver sensitivity (-74 dBm), $\|\mathbf{d}(t)\|$ is the relative distance between the UAV and the sensor node, $\lambda = c/f$ where f is the transmission frequency in Hz and $c = 3\times10^8$ m/s .[20] The received signal strength can be roughly characterized by direct propagated signal and the sum of reflection, diffraction, and scattering subsides.

In order to obtain the gradient for the heading controller, it is necessary to define a cost function that is an input to the extremum seeking step. With a single communication node, the cost function will be the SNR model itself used in Eq. (7), $J = SNR$. For multiple communication nodes, however, the cost function is defined with interactions between the multi-nodes, and it is necessary to satisfy the constraint. The straight forward method to define a figure of merit of the cost function is to calculate an average value by adding all of each SNR_i function with a proper weight value W_i

$$J_{opt} = \sum_{i=1}^{N} W_i SNR_i, \quad \text{and} \sum_{i=1}^{N} W_i = 1 \tag{34}$$

For decentralized control of multiple general N nodes, it is necessary to define relative cost functions between the node and UAV (UAV to ground node and UAV to UAV) for inputs to each extremum controller. Suppose we have two communication nodes (i, j) with two UAVs (l,m) and they are all in a liner network such that a node can send data to next neighbor node. Then, two relative cost functions are defined by

$$J_{i,l}(t) = SNR_{i,l}(\mathbf{p}_{i,l}(t)),\ J_{l,m}(t) = SNR_{l,m}(\mathbf{p}_{l,m}(t)),\ J_{m,j}(t) = SNR_{m,j}(\mathbf{p}_{m,j}(t)) \tag{35}$$

where $J_{i,l}$ is the SNR between the i ground node and UAV l, which is a function of the relative position vector $\mathbf{p}_{i,l}$ between them. Then, the cost function for the l vehicle is calculated by

$$J_l(t) = \begin{cases} \min\left(J_{j,l}(t), J_{l,m}(t)\right) & \left|J_{j,l}\right| > \varepsilon_{J_{j,l}} \ \&\ \left|J_{l,m}\right| > \varepsilon_{J_{l,m}} \\ \kappa_m \log\left(\dfrac{1}{J_{j,l}(t)} + \dfrac{1}{J_{l,m}(t)}\right) & \textit{otherwise} \end{cases} \tag{36}$$

Similarly, the cost function for the m vehicle is obtained by

$$J_m(t) = \begin{cases} \min\left(J_{l,m}(t), J_{m,j}(t)\right) & \left|J_{l,m}\right| > \varepsilon_{J_{l,m}} \ \&\ \left|J_{m,j}\right| > \varepsilon_{J_{m,j}} \\ \kappa_m \log\left(\dfrac{1}{J_{l,m}(t)} + \dfrac{1}{J_{m,j}(t)}\right) & \textit{otherwise} \end{cases} \tag{37}$$

The relative cost functions (J_l, J_m) are used as inputs for the self-estimating extremum controller for each vehicle.

IV. Autonomous Thermal Soaring for Long Flight Endurance Control

As mentioned previously, the UAVs that will be deployed as a part of this research require supplemental energy to extend endurance. To attain this increase, convective energy, or thermal updrafts, may be used to sustain flight. This section describes the process and conditions of thermal formation and presents the control functions of the autonomous soaring UAV as well as its implementation.

A. Thermal Formation and Conditions

Thermal updrafts are formed when the sun heats the ground. As a result of that process, the air immediately adjacent to the ground is also heated. This causes a difference in air density which results in the ascension of the lighter air. These rising parcels can occur as continuous columns or separate pockets and if found by a bird or glider pilot, can be used to gain altitude to extend flight[22, 25, 26] (see Fig. 5).

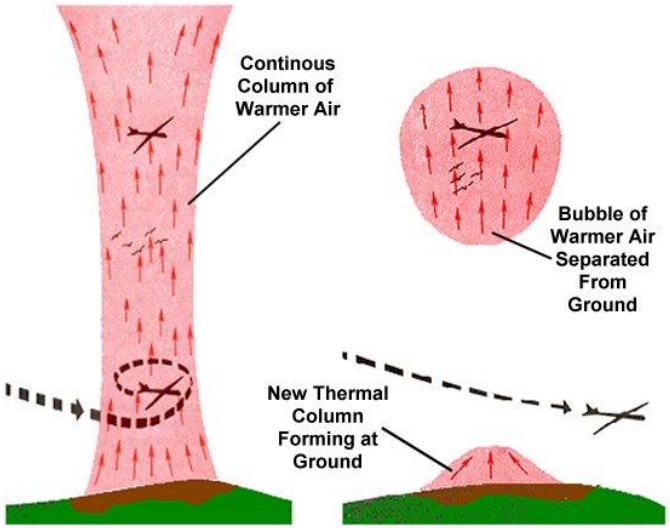

Figure 5 Types of thermals

Unfortunately, thermals are not ubiquitous. Nor are they guaranteed to reoccur in the same location and time (though they frequently do). Numerous conditions contribute to the formation of thermal lift, and though this paper mentions a few of them, it is by no means an exhaustive guide to thermal activity.

The basic requirement for thermal formation is solar radiation. It follows that thermals are directly dependent on surface heating, and are influenced by factors like topography. For example, on a cloud free day, an east facing slope is likely to produce thermals in the late-morning; whereas a west-facing slope will have more thermal activity in the late afternoon. Barring select exceptions, thermal lift is never present at night. Another place that consistently lacks thermal activity is over bodies of water. This is due to the high specific heat of water and its conductivity which leads heat away from the surface instead of warming the air above it. This also explains why most humid terrain, such as marshes and coniferous forests, are also poor producers of thermal lift; whereas dry ground tends to favor thermal activity. [25,26]

The lift provided by thermals offers an excellent opportunity for UAVs to improve endurance by sustaining continuous flight which is why it lends itself well to the purposes of the research presented in this paper. This approach is what normally is used by glider pilots to stay aloft. When an updraft is encountered the pilot begins to circle within the rising air, thus gaining altitude. When the desired altitude is reached or when the thermal no longer provides any useful lift, the pilot leaves the updraft and starts searching for a new one (Fig. 6).

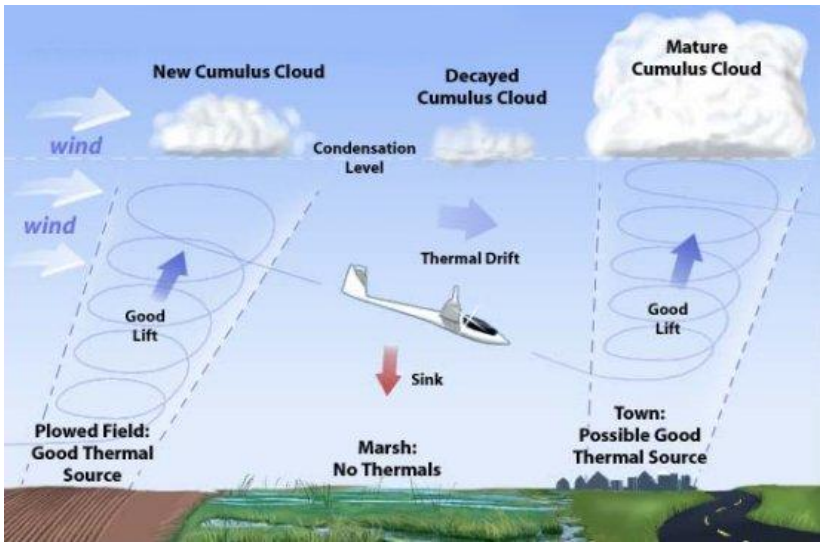

Figure 6 Thermal Soaring (aerospaceweb.org)

The major challenges for this kind of soaring flight are to find updrafts, and once one is found, to stay within it and try to center on it as accurately as possible to maximize climb rate.

B. Control of Soaring UAV

To enable a UAV to exploit thermal lift, a guidance and control method for the vehicle is needed. This was made possible through the use of the auto-soaring algorithm described below which was loosely based on the work of Allen.[26] It was implemented as follows: when switched to auto-soaring the flight is directed by the Simulink code, running on the onboard PC104. The code sends turn rate commands to the autopilot guiding the flight. In this case the glider will be either in search or soar mode. In search mode the UAV will follow a flight path defined by turn rate within the designated area. If the outer perimeter is reached, the UAV is turned back towards the designated area.

Auto-soaring algorithm

The algorithm has three central functions; search guidance, thermal detection, and thermal centering. The search guidance mode defines the flight path during search for lift and designates how the search for updraft is performed. The thermal detection mode monitors the energy rate of the aircraft and governs when to switch from search to soar mode and back. Once in soar mode, the thermal centering algorithm centers the vehicle in the updraft so as to gain altitude effectively.

Central to the detection of thermals, the triggering of soar-mode and the control of the UAV while tracking thermals is the vehicle's specific energy rate of change, $\dot{E}$, and specific energy acceleration, $\ddot{E}$. The vehicle's total energy E_{tot} (potential and kinetic) is given in Eq. (38) and is calculated using altitude h and airspeed V given by the static and dynamic pressure. The normalized energy E is given in Eq. (39).

$$E_{tot} = \frac{mV^2}{2} + mgh \tag{38}$$

$$E = \frac{E_{tot}}{mg} = \frac{V^2}{2g} + h \tag{39}$$

E is filtered to attenuate sensor noise in the input signals, and is then differentiated with respect to time to obtain normalized energy rate $\dot{E}$. This energy rate essentially represents the climb rate compensated for the exchange between potential and kinetic energy. The normalized energy rate is differentiated to obtain normalized energy acceleration $\ddot{E}$.

$$\dot{E} = \frac{V\dot{V}}{g} + \dot{h} \tag{40}$$

$$\ddot{E} = \frac{\dot{V}^2 + V \cdot \ddot{V}}{g} + \ddot{h} \tag{41}$$

Detection and Triggering of Soar-mode

To switch between soaring and search modes, $\dot{E}$ and $\ddot{E}$ are monitored to decide when a sufficiently strong thermal is entered and when to start circling in it. To accomplish this, the "Mode Logic" of Allen[11] was used (Fig. 7).

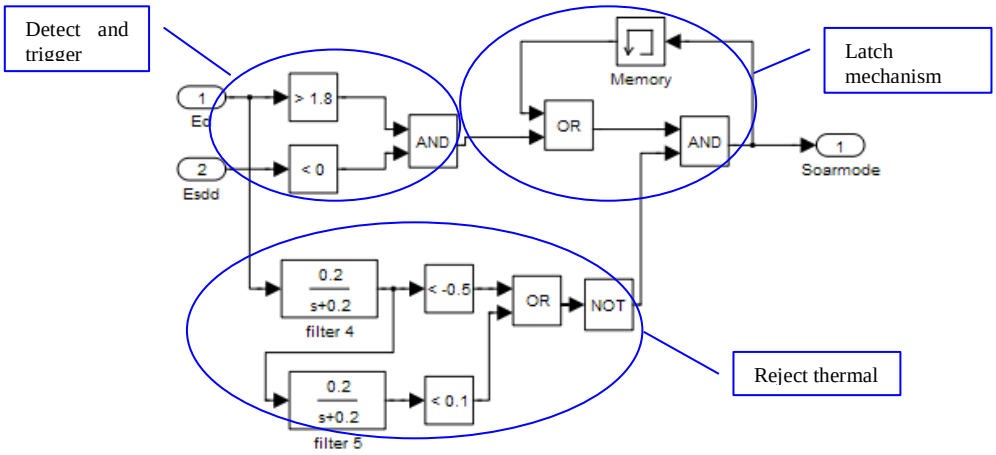

Figure 7 Diagram of Switching Control for Mode Logic, Search or Soaring

The "mode logic" block set has three functions:

- Trigger soar mode when $\dot{E}$ reaches a threshold value and $\ddot{E}$ becomes negative, which means the nearest point to the thermal center is reached.
- Latch on soar mode after it is triggered.
- Reject thermal when light sink is encountered for ~5 sec. or not enough lift is found in ~10 sec.

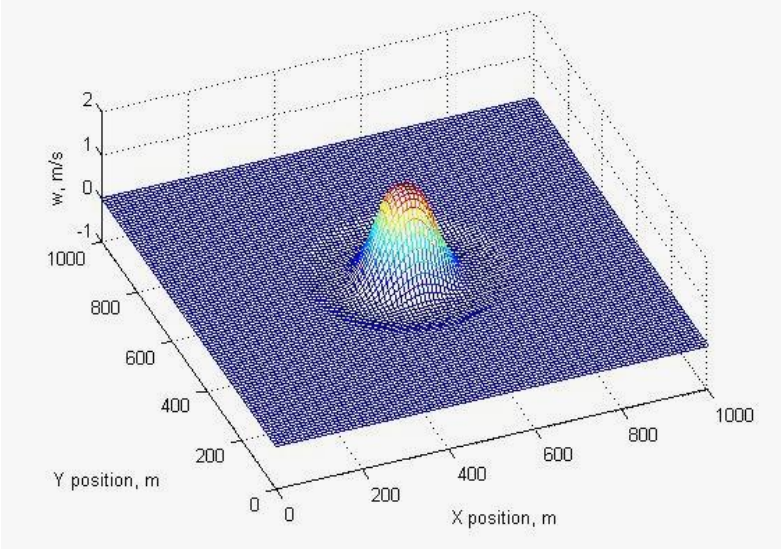

Figure 8 Example of Velocity Profile of an Updraft

Centering

Once a thermal is found, the next challenge is to stay within it and to effectively use lift to gain altitude. To achieve the best climb rate the center of the circular flight path needs to be adjusted so that it coincides with the core of the updraft. The radius of the flight path also needs to be tuned depending on the size of the thermal. The air usually rises faster in the center of the thermal gradually decreasing outwards and can even be surrounded by an area of a sink (Fig. 8). The area around the edges of the thermal is usually fairly turbulent.

Flying in the smallest possible radius would, therefore, seem to be the best strategy for soaring. However, smaller radius implies steeper bank angle, higher airspeed and an increase in sink rate of the air vehicle. To maximize the climb rate, a balance between bank angle and distance to the core of the thermal needs to be found.

The controller used for centering in this paper comes from the work of Andersson[35] and was derived from an efficient and widely used technique in manned aviation developed by thrice glider world champion Helmut Reichmann.[27] In his method, the bank angle is continuously adjusted depending on the change in climb rate as follows:

- As climb rate increases flatten the circle (~15-20° bank angle)
- As climb rate decreases steepen the circle (~50° bank angle)
- If climb rate is constant, keep constant bank (~25-30° bank angle)

This technique has the advantage of rapid centering while not being overly sensitive to latency in reacting to changes in thermal climb rate.

The method of Reichmann was employed as a base for the thermal centering controller used in this paper. It was realized by applying a feedback control law where the normalized energy acceleration $\ddot{E}$ was utilized to generate the turn rate command $\dot{\psi}_c$ to the onboard autopilot:

$$\dot{\psi}_c = \dot{\psi}_{ss} - k_1 \cdot \ddot{E} \tag{42}$$

where k_1 is the feedback gain and $\dot{\psi}_{ss}$ the steady state turn rate to maintain a constant climb rate.

In relation to Reichmann's technique, $\ddot{E}$ is utilized to provide a representation for changes in climb rate. To compensate for latency in the feedback due to lag in sensors and filtering of feedback signals Eq. (42) was modified to include a third term containing $\dddot{E}$, the controller is now given by

$$\dot{\psi}_c = \dot{\psi}_{ss} - k_1 \cdot \ddot{E} - k_2 \cdot \dddot{E} \tag{43}$$

where k_1 and k_2 are feedback coefficients. Fig. 9 shows the basic architecture of the thermal centering controller, where V is airspeed and P_{stat} static pressure for the vehicle.

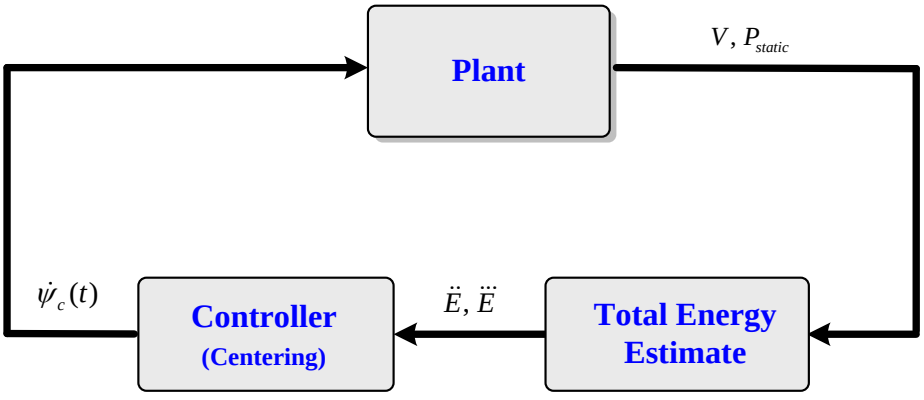

Figure 9 Diagram for Basic Function of The Feedback Centering Control

V. UAV Flight Systems

Discussed in this section are the aircraft chosen to conduct this research, a simulation model of that aircraft as well as the thermal updraft model used in the simulations.

A. Soaring Glider

The aerial platform used for the flight tests is based on an r/c cross country glider, the SBXC, produced by RnR Products[27] shown in Fig 10. Refer to Table 1 for more aircraft specifications. The aerial vehicle is further equipped with an electric motor and a folding propeller to facilitate easy take-off and regaining of altitude in case sufficient lift is not found. The motor will also be used for propulsion while in self-estimating extremum control mode. The UAV uses a Piccolo plus autopilot (Cloud Cap Technology)[28] for inner loop control, and the outer-loop autonomous soaring control runs on an onboard PC/104.[29] For communication between the UAV and a ground control center, a Wave Relay[30] is used. The control algorithms are coded in high-level programming language, Matlab/simulink[31].

Figure 10 The RnR SBXC Glider Used for Flight Experiments

Table 1 The Modified RnR SBXC Glider Specifications

Wing Span:	4.32 m (170")
Wing Area:	0.997 m^2 (1545 sq. in.)
Airfoil:	SD-2048
Aspect Ratio:	19.8:1
Weight:	6.55 kg (14.4 lb)
Wing Loading:	6.6 kg/m^2
Motor:	Plettenberg HP220

B. Communication Data Acquisition and Management System

In addition to a 900 MHz wireless link dedicated to the safe operation of multiple UAVs from the ground control station, a second wireless communication link, the Wave Relay networking systems operating at a 2.4 GHz 802.11 mesh network, was added to the aerial vehicle.[32] The radio is connected to a 3 dB omni-directional antenna mounted on the belly of the aerial robot for transmitting and receiving messages. Currently, the onboard PC-104 computer on the UAV is unable to extract the SNR value directly from the Wave Relay's management message. As such, the

SNR value will need to be extracted on the Linux machine located at the ground station and sent to the local host computer prior to transmission to the onboard computer. The information flow for the SNR from the ground pc to the UAV is illustrated in Fig 11. There is a switch on the local host computer which controls the type of SNR reading sent to the UAV. Currently, the switch caters for the following three types of SNR readings[9]: first, model-based SNR, This SNR reading is generated using the mathematical SNR model based on the current position and orientation of the UAV, second, This SNR reading is the actual SNR value computed by the Wave Relay radios, finally, This SNR reading is based on the mathematical SNR model modified by the updated actual SNR reading from the Wave Relay radios.

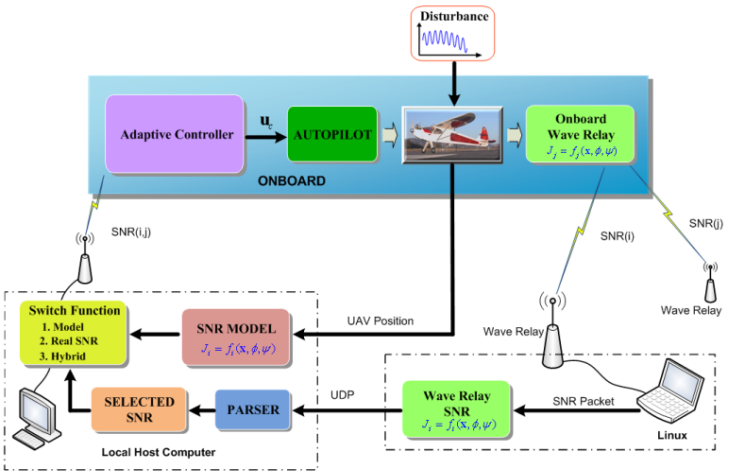

Figure 11 Flight Test Systems for Extremum Control based on SNR Data

C. Simulation Model of the Aircraft

In order to test and develop the algorithm a simulation model of the system was developed. All the coding and simulation was done in MATLAB/Simulink[31]. To get useful results, an accurate model to represent the aircraft was needed along with a way to simulate the thermal updrafts.

To model the air craft described above, a six degree of freedom (6DoF) model of the UAV in Simulink was generated. This required a number of aerodynamic/stability and control derivatives together with the mass moments of inertia with respect to the principal axis of the aircraft. The necessary aerodynamic and control derivatives were calculated using two different software packages, AVL[33] and Linair[34]. Both programs are based on the vortice lattice method and require the physical geometry of the air vehicle as an input file.

In order to obtain an accurate model, the moments of inertia were experimentally obtained[23]. This was done by suspending the aircraft and letting it swing as a pendulum around the three principal axes (one at a time).

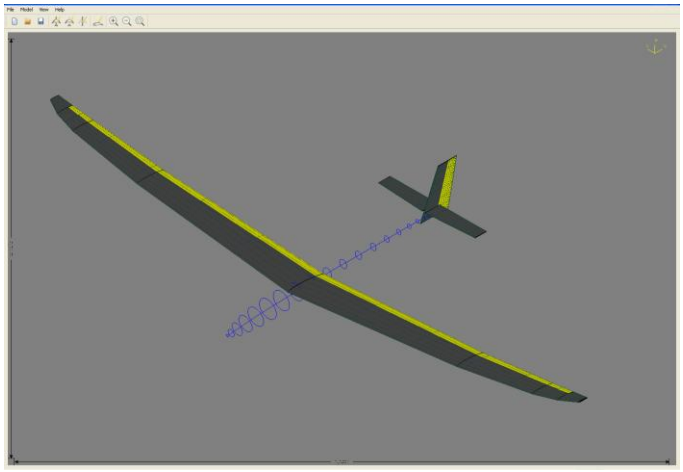

Figure 12 AVL-Model of the UAV

D. Updraft Model of the Aircraft

Thermal updrafts are known to vary greatly in size and shape and are therefore difficult to model accurately. However to be able to simulate the auto-soaring code, a model of thermals was needed. An updraft model developed at NASA Dryden Flight Research Center was used to model the updrafts used for the simulations[24]. An example of an updraft field created by the model is displayed in Fig. 13 below.

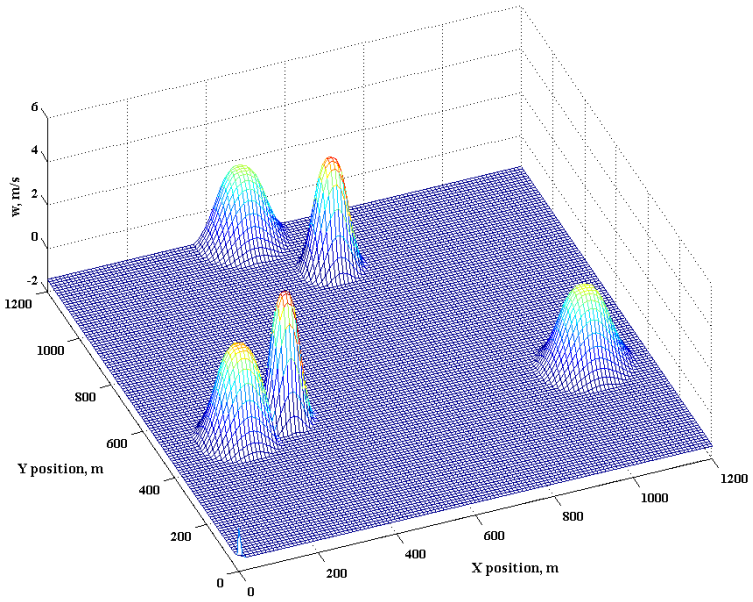

Figure 13 Updraft Field Created with the NASA Dryden Updraft Model

VI. Flight Test and Simulation Study

Flight experiments and simulations were performed with two static communication nodes relaying by a single autonomous soaring UAV. First, the guidance control for the self estimating extremum control of an aerial vehicle for maximum communication throughputs was tested in real flight experiment for robustness and effectiveness capabilities. Second, the integrated hybrid control algorithm with high endurance flight control technique is evaluated through simulation studies. While in simulation studies extended flight endurance of the soaring UAVs makes the communication and data relay mission more effective and robust compared to that of the conventional aerial platforms.

A. Flight Test for Self-Estimating Extremum Control

The real-time adaptive optimization algorithm which integrates an extremum-seeking algorithm with a gradient-based controller to obtain an optimal UAV loitering posture to maximize communication links quality between one UAV and two transmitting ground nodes is presented first. The communication links flight test was conducted as part of the TNT experimentation program (TNT-09-01) at McMillan Air Field in Camp Roberts, California on November 20, 2008. The test was conducted with two stationary ground nodes and the Rascal UAV. The two ground nodes depicted in Fig. 7 acted as the command station and the survey vehicle while the UAV functioned as the relay vehicle. The primary objective was to validate the designed onboard adaptive optimization algorithm that would drive the Rascal UAV to an optimal loitering flight path and maximize the SNR between the two nodes and the UAV.

Additionally, the aerial vehicle is equipped with 2.2 dB omni-directional antenna (HG2402RD-RSF). The location of the sensor nodes and terrain of the air field is shown in Fig 14. Figure 15 shows the flight trajectory of

the UAV during the test. Initially, the UAV was in a holding pattern orbiting north of the GCS node. When the control algorithm was activated, the UAV started to move in the direction of the steepest increase in the SNR value. When the UAV reached the region of peak SNR, a steady-state heading command was passed to make the UAV orbit around the optimal point. It was observed that the orbit around the optimal point was elongated and not a circular path. The circular lines shown in Figure 15 are contour lines of constant SNR generated from the static SNR map in east-north coordinates for a stationary (non-dynamic) UAV with fixed altitude, heading, and bank angle.

Figure 14 Relative Location of the GCS node and Remote Node [From Google Earth]

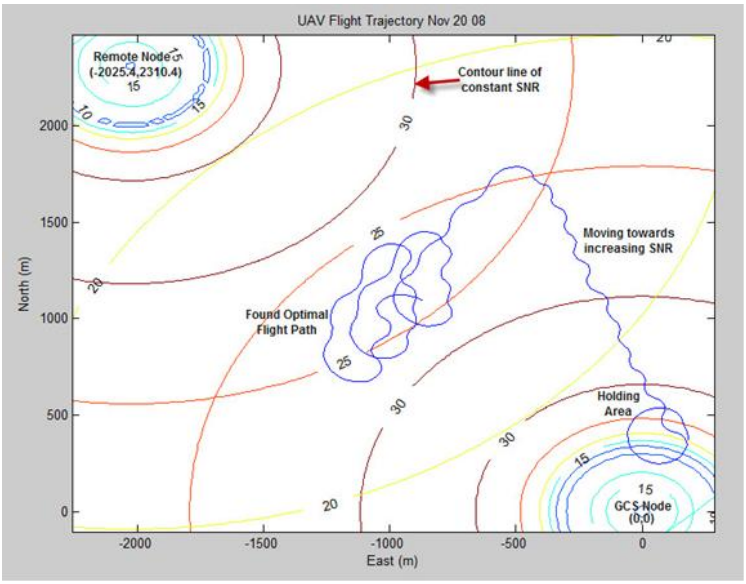

Figure 15 UAV Flight Path during the TNT Experimental Program

Figure 16 shows the error between the actual data and simulated one from the SNR model. It is seen that the simulated SNR compared nicely with the actual SNR data from the flight test. The error of the simulated model with respect to the actual SNR data was within 15% except for the holding area where the error was more than 30%. The

holding area is near the GCS node and the model is not accurate at this near range. Hence, the simulated SNR reading between the GCS and UAV tends to show a large error in the holding area.

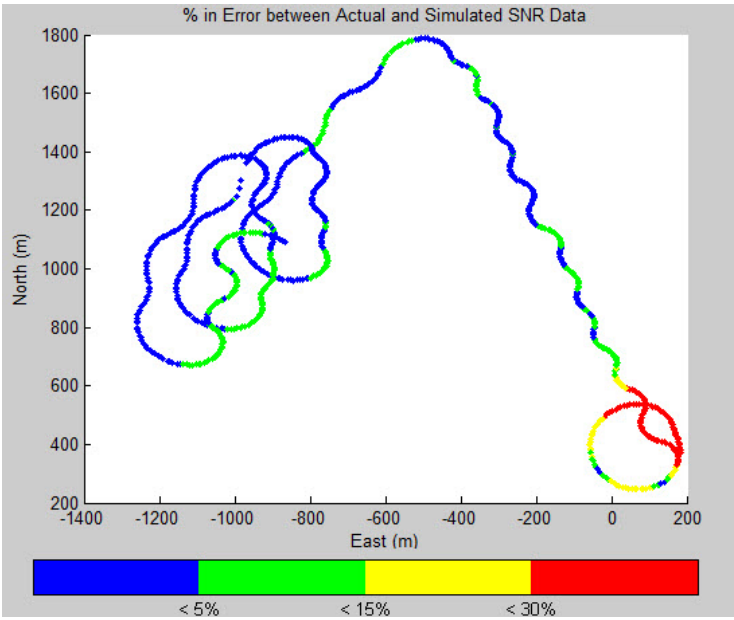

Figure 16 SNR Error (in %) between Simulated Reading and Actual Flight Test Data

B. Simulation Study for Hybrid Control of Robust Communication Networks

In this section, the performance of the proposed hybrid control algorithms for robust high bandwidth wireless communication relay functionality is demonstrated. The simulation study is composed of two phases; one is the high bandwidth communication links between multiple nodes where the self-estimating extremum control technique is executed to find an optimal trajectory of a relay UAV. The other phase is the soaring mode where an onboard soaring control algorithm is executed to search updraft thermal energy to extend the endurance of the aerial vehicle with a specified spiral searching pattern as described in Fig. 3.

Figure 17 describes the location of an example thermal updraft used in the simulations. The location is 300 m east and 470 m north.

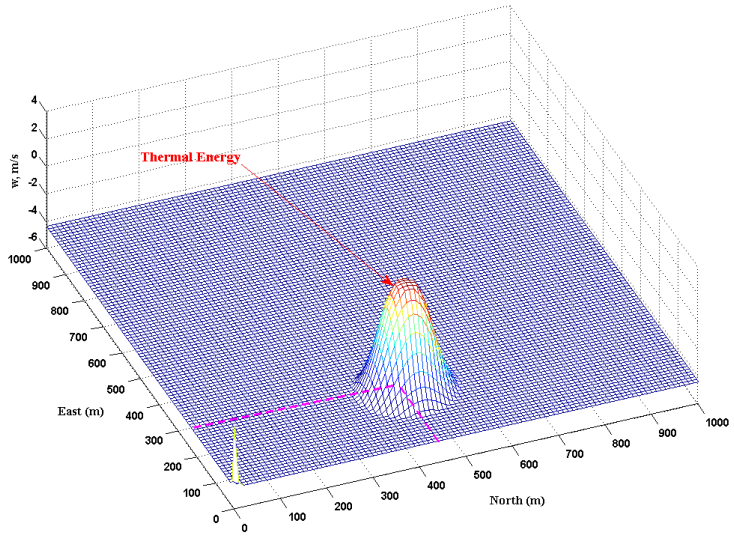

Figure 17 Location of Updraft Thermal Energy

In Fig. 18, the trajectories of a soaring aerial vehicle are shown, which are generated from the hybrid supervisory control technique with application to the communication networking problem with two sensor nodes. It is assumed that there is no packet loss and time delay effects on the communications among the nodes. The optimal location of the UAV is obtained by using the self-tuning extremum control resulting in converging to the line-of-sight intersection line (400 in north and 200 in east) between the two communication nodes. After the optimal communication links is established near to the optimal location, the second mode of the thermal searching is executed to find an updraft thermal energy to extend the endurance of the aerial vehicle. As can be seen in the Fig. 18, the UAV found a thermal energy, located in 470 m north and 300 m east, with a spiral flying pattern.

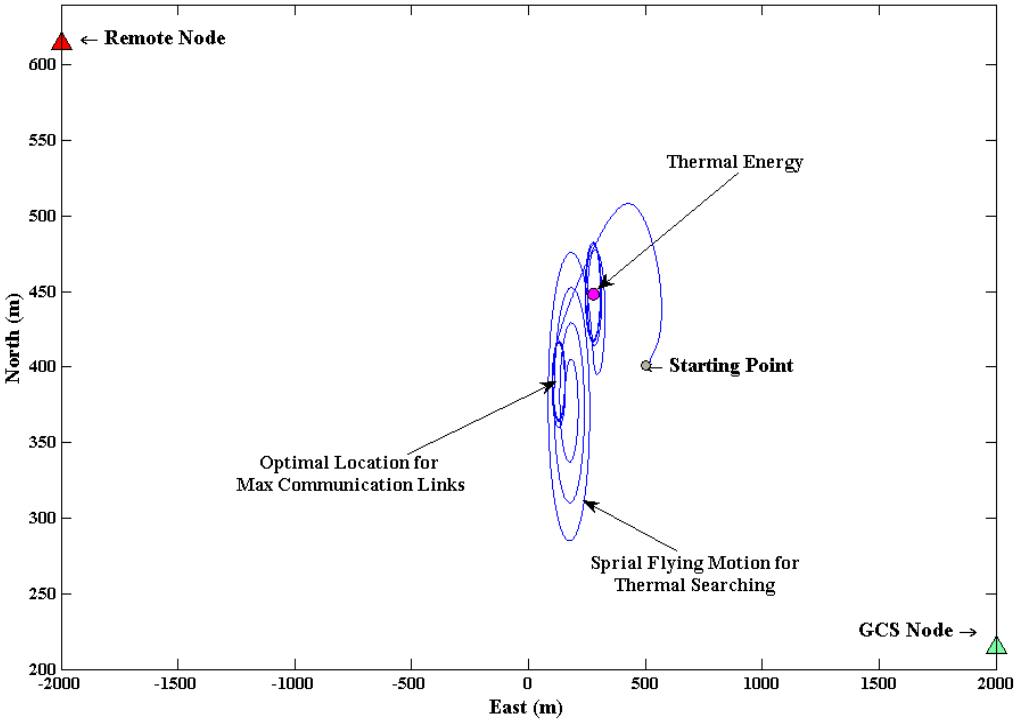

Figure 18 Plot of Hybrid Control for Robust Communication Networks Using Long-Endurance UAV

Fig. 19 illustrates the variation of the total SNR cost value along with the trajectories of the soaring UAV. It is seen that the UAV reached an optimal location in 50 sec providing the maximum 32.5 dB SNR value. On the other hand, a thermal searching mode was executed around 30 sec later to extend endurance using a thermal updraft. After the soaring UAV found the thermal, the communication strength was drop to 32 dB, which satisfies the minimum threshold value. Figure 20 describes the time rate of change of the SNR cost function in time where it is seen that the optimal location for high bandwidth communication links was established around 50 sec after the self-estimating extremum control algorithms were executed, and the UAV found a thermal energy 220 sec later. In this way, the soaring UAV could establish the robust and maximum communication networks while the endurance of the small UAV could be extended dramatically, usually from 2 hours to more than 6 hours.

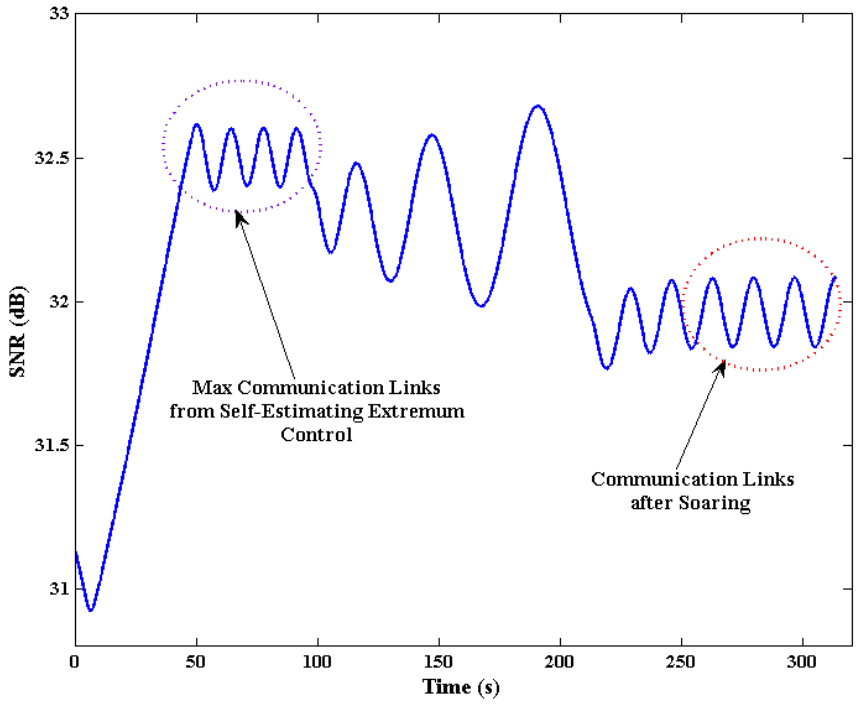

Figure 19 Plot of the Variation of SNR Value as Figure-of-Merit Cost

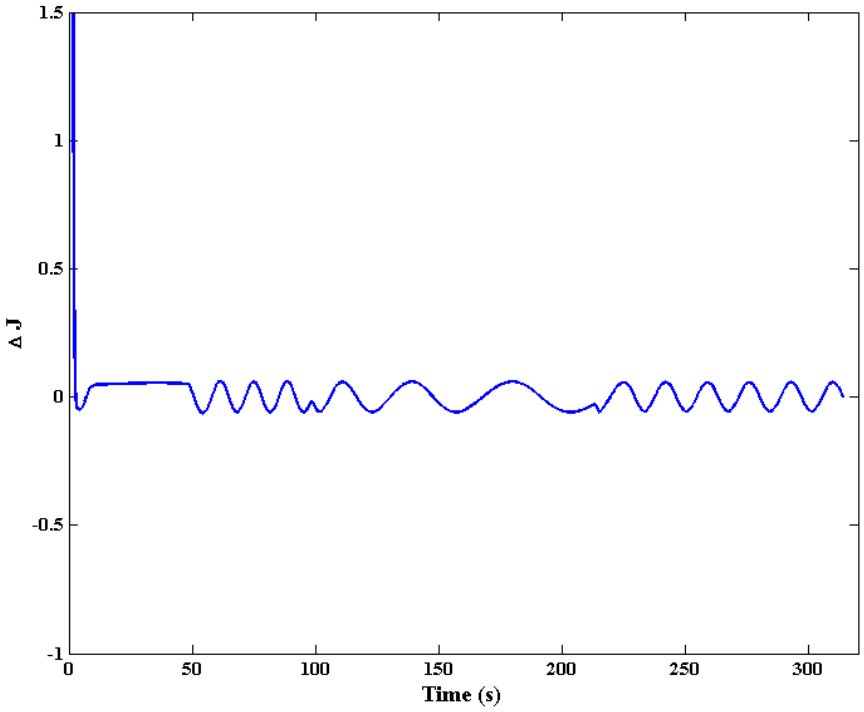

Figure 20 Plot of the Time Rate of Change of SNR Cost Function

VII. Conclusions

In this paper, a hybrid control is developed by integrating the self-estimating extremum controller for a high bandwidth communication relay with the long-endurance flight controller for a soaring technique for maximum flight endurance. The developed self-estimating control algorithms which drive the UAV to reposition itself autonomously in order to maintain an optimal loitering flight path to achieve the optimal communication link quality between two transmitting ground nodes is validated through the real flight experiment. In addition, the integrated hybrid control architecture embedded with the soaring control algorithm for the high flight endurance is evaluated through simulation studies. Extended flight endurance obtained by utilizing the soaring flight control techniques makes the communication and data relay mission more effective and robust compared to that of the conventional aerial platforms.

Acknowledgments

This work was supported by USSOCOM under NPS-SOCOM TNT cooperative and the Office of Naval Research (ONR).

References

[1] D. A. Schoenwald, "AUVs: In Space, Air, Water, and on the Ground," IEEE Control Systems Magazine, vol. 20, no. 6, pp. 15–18, Dec. 2000.

[2] I J. Cortes, S. Marinez, T. Karatas, F. Bullo, "Coverage Control for Mobile Sensing Networks," IEEE Transactions on Robotics and Automation, vol. 20, no. 2, pp. 243–255, April 2004.

[3] Maj. F. J. Pinkney, D. Hampel, and S. DiPierro, "Unmanned Aerial Vehicle Communications Relay", *in Proceedings of the IEEE*, pp.47-51, 1996.

[4] S. Oh, L. Schenato, P. Chen, and S. Sastry, "Tracking and Coordination of Multiple Agents Using Sensor Networks: System Design, Algorithms and Experiments", *in Proceedings of the IEEE*, vol. 95, no. 1, pp.234-254, Jan. 2007.

[5] P. Basu, J. Redi, and V. Shurbanov, "Coordianted Flocking of UAVs for Improved Connection of Mobile Ground Nodes", *in Proceedings of the IEEE Military Communications Conference*, pp.1628-1634, 2004.

[6] Cory R. Dixon and Eric W. Frew, "Cooperative Electronic Chaining Using Small Unmanned Aircraft," AIAA 2007 Conference and Exhibit, 2007.

[7] P Zhan, K. Yu, and A. Lee Swindlehurst, "Wireless Relay Communication Using an Unmanned Aerial Vehicle," IEEE 7th Workshop on Signal Processing Advances in Wireless Communications, 2006.

[8] E. W. Frew, T. X. Brown, "Airborne Communication Networks for Small Unmanned Aircraft Systems," *Proceedings of the IEEE*, vol. 96, no.12, Dec. 2008.

[9] D.-J. Lee, K. Kam, I. Kaminer, D. P. Horner, A. Healey, S. Kragelund, K. Andersson, and K. Jones, "Wireless Communication Networks between Distributed Autonomous Systems Using Self-Tuning Extremum Control," AIAA Unmanned Unlimited Conference, Seattle, WA, April 6-9, 2009.

[10] Mark B. E. Boslough, "Autonomous Dynamic Soaring Platform for Distributed Mobile Sensor Arrays," SAND Report, 2005, SAND2002-1896.

[11] M. Allen, V. Lin. *Guidance and Control of an Autonomous Soaring UAV*, Edwards, CA, 2007, NASA/TM-2007-214611/REV1.

[12] K. Andersson, I. Kaminer, K. D. Jones, V. Dobrokhodov, and D.-J. Lee, "Cooperating UAVs Using Thermal Lift to Extend Endurance," AIAA Unmanned Unlimited Conference, Seattle, WA, April 6-9, 2009.

[13] J. W. Langelaan, "Biologically Inspired Flight Techniques for Small and Micro Unmanned Aerial Vehicles," *in AIAA Guidance, Navigation and Control Conference and Exhibit*, Honolulu, Hawaii, Aug. 18-21 2008.

[14] R. Barate, S. Doncieux, and J.-.A Meyer, "Design of a Bioinspired Controller for Dynamic Soaring in a Simulated Unmanned Aerial Vehicle," *Bioinspiration and Biomimetics*, Vol. 1, 2006, pp. 76-88.

[15] D. J. Edwards, "Implementation Details and Flight Test Results of an Autonomous Soaring Controller," *in AIAA Guidance, Navigation and Control Conference and Exhibit*, Honolulu, Hawaii, Aug. 18-21 2008.

[16] Kartik B. Ariyur and Miroslav Krstic, *Real-Time Optimization by Extremum-Seeking Control*, Wiley-Interscience publication, 2003.

[17] J. Sternby, A Review of Exremum Control, Technical Report, Department of Automatic Control, Lund Institute of Technology, April 1979.

[18] A. Quarteroni, R. Sacco, and F. Saleri, *Numerical Mathematics*, New York, NY, Springer-Verlag, Inc., 2002.

[19] R. N. Banavar, D. F. Chichka and J. L. Speyer, "Convergence and Synthesis Issues in Extremum Seeking Control," *Proceedings of the American Control Conference*, Chicago, Illinois, pp. 438-443, June 2000.

[20] T. S. Rappaport, "Wireless Communications : Principles and Practice," 2nd ed.Upper Saddle River, N.J: Prentice Hall PTR, 2002.

[21] C. E. Shannon, "Communication In The Presence Of Noise, " Proceedings of the IEEE, vol. 86, pp. 447-457, 1998.
[22] H. Reichmann, "Cross-Country Soaring," Soaring Society of America, Inc., 1993, ISBN 1-883813-01-8.
[23] M. P. Miller, "An Accurate Method of Measuring the Moments of Inertia of Airplanes," (NACA technical note no.351)
[24] M. Allen, "Updraft Model for Development of Autonomous Soaring Uninhabited Aerial Vehicles," AIAA Aerospace Sciences Meeting and Exhibit, Reno, Nevada, Jan 9-12, 2006, AIAA-2006-1510.
[25] R. Axelsson and R. Danewid, "Segelflyg: en lärobok," Segelflygsport Förlag, 2002, ISSN 91-973848-3-6.
[26] D. Pagen, "Understanding the sky," Sport Aviation Pubns, Feb 1992.
[27] RnR Products, available at http://www.rnrproducts.com/ [cited 10 Aug. 2008].
[28] "Piccolo Documentation," http://www.cloudcaptech.com [cited 15 July 2008].
[29] Microspace PC-104," http://www.adlogic-pc104.com [cited 25 June 2008].
[30] "Wave Relay QUAD Radio Router," available at http://www.persistentsystems.com/products/ [cited 20 July 2008].
[31] MATLAB/Simulink, Ver.7.1, The MathWorks, Inc.
[32] K. D. Jones, V. Dobrokhodov, I. Kaminer, D.-J. Lee, E. Bourakov, M. R. Clement, "Development, System Integration and Flight Testing of a High-Resolution Imaging System for Small Unmanned Aerial Systems," in *47th AIAA Aerospace Sciences Meeting*, Orlando, Florida, Jan. 5-8 2009.
[33] AVL, Athena Vortex Lattice, Ver.3.26, URL: http://web.mit.edu/drela/Public/web/avl/avl_doc.txt [cited 10 Mar 2009]
[34] LinAir v3.4, Desktop Aeronautics, Stanford, CA